Acta Crystallographica Section B
Structural Science
ISSN 0108-7681

Structures and phase transitions in the ordered double perovskites $Ba_2Bi^{III}Bi^{V}O_6$ and $Ba_2Bi^{III}Sb^{V}O_6$

Brendan J. Kennedy,[a] Christopher J. Howard,[b,c]* Kevin S. Knight,[d] Zhaoming Zhang[b] and Qingdi Zhou[a]

[a]School of Chemistry, University of Sydney, Sydney, NSW 2006, Australia, [b]Australian Nuclear Science and Technology Organisation, Private Mail Bag 1, Menai, NSW 2234, Australia, [c]School of Physics, University of Sydney, Sydney, NSW 2006, Australia, and [d]ISIS Facility, Rutherford Appleton Laboratory, Chilton, Didcot, Oxfordshire OX11 0QX, England

Correspondence e-mail: cjh@ansto.gov.au

Received 13 November 2005
Accepted 22 May 2006

High-resolution neutron powder diffraction has been used to investigate the structures and phase transitions in the double perovskites $Ba_2Bi^{3+}Bi^{5+}O_6$ (dibarium dibismuth hexaoxide) and Ba_2BiSbO_6 (dibarium bismuth antimony hexaoxide) in the temperature ranges 4.2–973 and 4.2–625 K, respectively. The charge-ordered bismuthate adopts four structures in the temperature range – monoclinic in $P2_1/n$, monoclinic in $I2/m$, rhombohedral in $R\bar{3}$, and finally cubic in $Fm\bar{3}m$. The low-temperature monoclinic structure has been determined for the first time. The transitions from $P2_1/n$ to $I2/m$, at 132 K, and $R\bar{3}$ to $Fm\bar{3}m$, at 820 K, are tricritical in nature; the transition from $I2/m$ to $R\bar{3}$ at *ca* 430 K is discontinuous. The behaviour of Ba_2BiSbO_6 is very similar, except that the transition temperatures are lower – 250 K for $I2/m$ to $R\bar{3}$ and 515 K for $R\bar{3}$ to $Fm\bar{3}m$ – and the low-temperature structure is not formed at all. The $R\bar{3}$ to $Fm\bar{3}m$ transition in this compound is closer to second order in nature, although there is evidence for some contribution from higher-order terms.

1. Introduction

The structures and phase transitions in the perovskite $BaBiO_3$ have attracted interest since the discoveries of superconductivity in the systems $BaBiO_3$–$BaPbO_3$ (Sleight *et al.*, 1975) and $BaBiO_3$–$KBiO_3$ (Cava *et al.*, 1988). It has been established (Cox & Sleight, 1976*a*) that $BaBiO_3$ is not the simple perovskite its formula might suggest, but instead an ordered double perovskite, the two different *B*-site cations being distinguished by charge rather than by elemental species. This is acknowledged by writing its formula as $Ba_2Bi^{III}Bi^{V}O_6$ or $Ba_2Bi^{3+}Bi^{5+}O_6$. The charge ordering accounts for the fact that $BaBiO_3$ is electrically semiconducting rather than metallic as otherwise would be expected. Charge ordering in $BaBiO_3$ persists to high temperatures (Cox & Sleight, 1976*a*; Zhou & Kennedy, 2004), although it is thought to be destroyed by the substitution at modest levels of Pb for Bi (Cox & Sleight, 1976*b*) or K for Ba (Pei *et al.*, 1990).

$BaBiO_3$ undergoes a number of temperature-induced phase transitions associated with BiO_6 octahedral tilting. Cox & Sleight (1976*a*, 1979) reported the structure to be monoclinic in $I2/m$ at room temperature and to show a first-order transition to rhombohedral in $R\bar{3}$ at *ca* 405 K followed by a continuous transition to cubic in $Fm\bar{3}m$ at *ca* 750–800 K. Pei *et al.* (1990) extended the study to low temperatures and reported an apparently continuous transition at *ca* 140 K to a primitive monoclinic structure on the same cell as the body-centred monoclinic structure seen at room temperature. These reports were reviewed by Howard *et al.* (2003), who consid-

ered the sequence of transitions in $Ba_2Bi^{3+}Bi^{5+}O_6$ as likely to be

~ 140 K		405 K		750-800 K	
Monoclinic	---------->	Monoclinic	---------->	Rhombohedral	----------> Cubic,
$P2_1/c$ $(a^+b^-b^-)$		$C2/m$ $(a^0b^-b^-)$		$R\bar{3}$ $(a^-a^-a^-)$	$Fm\bar{3}m$ $(a^0a^0a^0)$
	Continuous		Discontinuous		Continuous

consistent with the scheme developed from their group theoretical analysis.[1] Subsequently, Zhou & Kennedy (2004) completed a synchrotron X-ray study of $BaBiO_3$ from room temperature to 923 K. They confirmed that the monoclinic to rhombohedral transition was discontinuous and found the rhombohedral to cubic transition to be second order. Zhou & Kennedy reported the temperatures as 425 and 893 K for the monoclinic to rhombohedral and rhombohedral to cubic transitions, respectively.

In this paper we report the results from a very-high-resolution neutron powder diffraction study of $BaBiO_3$ at temperatures in fine steps from 4 to 973 K. The structure at low temperatures has been determined for the first time and all the phase transitions have been followed in detail. A notable feature of the diffraction studies of the charge-ordered double perovskite $Ba_2Bi^{3+}Bi^{5+}O_6$ is that in neutron diffraction there can be no contrast in scattering between Bi^{3+} and Bi^{5+}, and the contrast is negligible in X-ray diffraction as well. The superlattice (cell doubling, or *R*-point, see Howard *et al.*, 2003) reflections that normally result from such contrast depend instead on the contrast in scattering between $Bi^{3+}O_6$ and $Bi^{5+}O_6$ octahedra. This in turn depends on differences in oxygen positions due to the size difference between Bi^{3+} and Bi^{5+}, the radii of these ions being 1.03 and 0.76 Å, respectively (Shannon, 1976). Since the contrast depends entirely on the movements of O atoms, and also given the presence in this compound of much heavier elements, an investigation by neutron rather than X-ray diffraction is to be preferred.

We also report results from an analogous study of the more conventional, chemically distinguished, double perovskite Ba_2BiSbO_6 ($Ba_2Bi^{3+}Sb^{5+}O_6$). At room temperature this is known to adopt the same structure (monoclinic in $I2/m$) as $BaBiO_3$ (Thornton & Jacobson, 1978). We find this undergoes a quite similar sequence of temperature-induced phase transitions, although the transition temperatures are lower in Ba_2BiSbO_6 than in $BaBiO_3$ and the $P2_1/n$ monoclinic structure is not seen at all. The differences are attributable to the smaller (average) size of cations on the *B* site when Sb^{5+} (ionic radius 0.60 Å) replaces the larger Bi^{5+} ion.

2. Experimental and data analysis

The polycrystalline samples of $BaBiO_3$ and Ba_2BiSbO_6 were prepared by the high-temperature solid-state reaction of stoichiometric quantities of $BaCO_3$ (99.98%, Aldrich), Sb_2O_3 (99.99%, Aldrich) and Bi_2O_3 (99.999%, Aldrich). For $BaBiO_3$ the preparation involved heating at 1073 K over a total of 480 h, with cooling every 48 h and regrinding to promote sample homogeneity. For Ba_2SbBiO_6, the sample was heated for 20 h each at 1073, 1123, 1173 K and, finally, 1223 K, with cooling and regrinding after every heating step. Powder patterns recorded using a Shimadzu XRD-6000 diffractometer and Cu $K\alpha$ radiation were used to provide a check on crystallinity and the phase purity of the products.

Neutron diffraction data were recorded using the high-resolution powder diffractometer (HRPD) at the ISIS neutron facility, Rutherford Appleton Laboratories, UK (Ibberson *et al.*, 1992). The temperature ranges of interest, for $BaBiO_3$ from 4.2 to 973 K, and for Ba_2BiSbO_3 from 4.2 to 625 K, necessitated the use of both cryostat and furnace. For measurements in the cryostat, the powdered sample was lightly packed into an aluminium can of slab geometry, area 20 × 20 mm, 15 mm thick, with thin neutron-transparent windows front and back. Heat was supplied to the sample through a 100 W cartridge heater inserted in the side wall of the sample can and temperature was monitored using a Rh/Fe sensor located in the opposite wall. A gadolinium, neutron-absorbing mask was attached to the side of the can facing the incident beam and back-scattering detectors to prevent contaminant Bragg peaks arising from either the body of the sample can, including sensor or heater, or the stainless steel frames supporting the vanadium windows. The assembly was attached to a centre-stick and mounted in an AS Scientific, 50 mm diameter, 'Orange' helium cryostat, located at the 1 m position of the diffractometer. The exchange gas was He at 30 mbar. For the furnace work, the sample was loaded into an 11 mm diameter sample can, which was then mounted in the RAL vacuum furnace. This furnace has vanadium heating elements, and the thermometry is based on type-K thermocouples positioned in contact with the sample can at about 20 mm above the beam centre. The sample temperature was controlled to ±0.2 K. Diffraction patterns from the sample, whether in the cryostat or furnace, were recorded over the time-of-flight range 30–130 ms in both back-scattering and 90° detector banks, corresponding to *d* spacings from 0.6 to 2.6 and from 0.9 to 3.7 Å, respectively. The patterns were normalized to the incident beam spectrum, as recorded in the upstream monitor, and corrected for detector efficiency according to prior calibration with a vanadium scan. For $BaBiO_3$, the cryostat was used for temperatures from 4.2 to 400 K, then the furnace used for a measurement at room temperature followed by measurements from 373 to 973 K. For Ba_2BiSbO_6, the cryostat was used for measurements from 4.2 to 385 K, then the furnace for measurements at room temperature, and from 375 to 625 K. The temperature intervals were typically 10 K, but varied from 5 to 25 K depending on the proximity to phase transitions. Most patterns were recorded to a total incident proton beam of *ca* 8 μA h, corresponding to approximately 15 min of data collection, sufficient to give a good determination of lattice parameters and reasonable estimates of the internal coordinates. Longer counting times, in the range 35–70 μA h were used for $BaBiO_3$ at 4.2, 50, 100, 150, 200 and 498 K and for Ba_2BiSbO_6 at 4.2

[1] It is usually more convenient to describe the monoclinic structures on alternate cells, such that the space groups (tilt systems) for the (proposed) low-temperature and room-temperature structures read $P2_1/n$ ($a^-a^-c^+$) and $I2/m$ ($a^-a^-c^0$), respectively.

and 325 K so as to provide superior structure determinations in the temperature ranges of interest.

In the first instance, the different phases were identified by a close inspection of the diffraction patterns, paying particular attention to peak splittings and the presence or absence of the various superlattice peaks (Howard *et al.*, 2003). Inspection of a selection of diffraction patterns from $BaBiO_3$ (Fig. 1) serves to illustrate this procedure. The main peaks have been indexed on the basis of the parent or pseudo-cubic cell. The structure has been taken as cubic when all are single peaks, rhombohedral when the pseudo-cubic 222 is split but not the 200, and monoclinic when both the 200 and 222 (among others) show splitting. The superlattice peaks also are indexed on the basis of the pseudo-cubic cell, and marked as *R* point (half-integral indices), *M* point (one integral, two half-integral indices) or *X* point (two integral indices, one half-integral). Intensities at the *R* points arise from *B*-site cation ordering and/or out-of-phase (−) octahedral tilting, intensities at the *M* points from in-phase (+) octahedral tilting, and intensities at the *X* points simply from the combination of *R*- and *M*-point distortions. From inspection of these patterns (Fig. 1), and considering only those possibilities enumerated by Howard *et al.* (2003), the identification of structures becomes relatively straightforward. Based on the initial identifications, both lattice parameters and atomic coordinates were determined, using the Rietveld method as implemented in the *GSAS* computer program (Larson & Von Dreele, 2000; Toby, 2001). Patterns from both the back-scattering and the 90° detector banks were fitted simultaneously, the diffractometer constant for the 90° bank being released to ensure that the lattice parameters were determined by the higher-resolution back-scattering bank in every case. The diffractometer constants used in the furnace run were slightly adjusted so that the lattice parameters obtained in the furnace matched those obtained in the cryostat in the overlapping temperature range. Such an adjustment was justified on the grounds that the diffractometer constants depend on the precise positioning of the sample, which would be different in the furnace as compared with in the cryostat. Internal coordinates were refined along with the displacement parameters, the oxygen displacement parameters taken to be anisotropic in the higher-symmetry rhombohedral and cubic structures. The isotropic displacement parameters for the two *B*-site cations, Bi^{3+} and Bi^{5+} or Bi^{3+} and Sb^{5+} in $BaBiO_3$ and Ba_2BiSbO_6, respectively, were in many cases constrained to be equal. Apparent from the recorded patterns were regions of co-existence of the monoclinic *I*2/*m* and rhombohedral $R\bar{3}$ phases, from *ca* 433 to 443 K in $BaBiO_3$ and from 245 to 255 K in Ba_2BiSbO_6. Two-phase refinements were attempted in these regions, without success in the case of Ba_2BiSbO_6, but with more success in $BaBiO_3$ where the distortions of the unit cell are larger and thus the diffraction patterns from the two co-existing phases more readily distinguished.

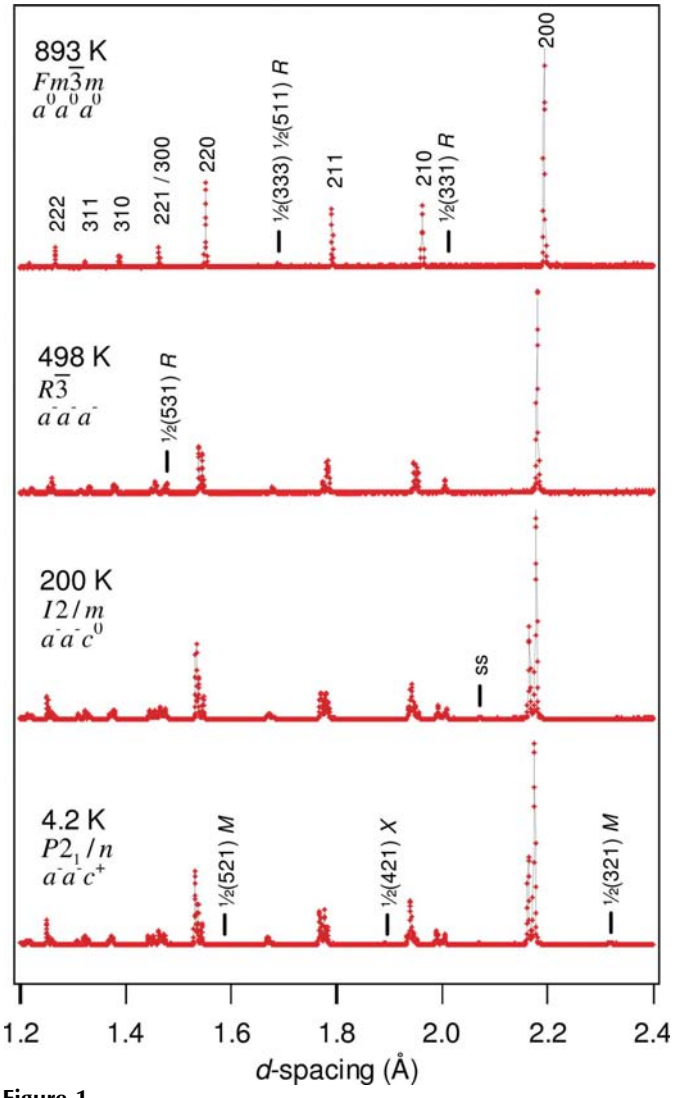

Figure 1
Extracts ($1.2 < d < 2.4$ Å) from the diffraction patterns recorded in the back-scattering detectors from $BaBiO_3$ in each of its four phases. Crosses represent the observed data. The peaks are indexed on the parent perovskite (*ca* 4 Å) cell. The peaks with fractional indexing are superlattice peaks arising from cation ordering (or rather the associated oxygen displacements) and/or BiO_6 octahedral tilting. The low-temperature patterns show a weak contaminant peak from stainless steel (ss). The structures were identified from the main-peak splittings and the presence or absence of superlattice peaks. The continuous lines are fits obtained by the Rietveld method assuming the indicated structures.

Obtaining good values for the internal coordinates proved to be more difficult than anticipated, especially when refining from the 8 μA h (*ca* 15 min) patterns. One problem is clear from Fig. 1: The contributions at the *R* points from cation ordering in $BaBiO_3$ (that is the contrast between the $Bi^{3+}O_6$ and $Bi^{5+}O_6$ octahedra) are, as evident in the pattern from the cubic phase, quite small, and in the lower-symmetry structures they are largely swamped by contributions from octahedral tilting. In addition, if one solution is obtained, a second solution corresponding to interchanging Bi^{3+} and Bi^{5+} can be obtained by a rather small displacement of O atoms. The implication is that the least-squares residual should have two equal minima in close proximity (in parameter space) to each other. In the event of noisy data it is reasonable to expect that additional minima – false minima – may occur in the near vicinity of the true ones. Indeed we encountered such minima in our refinements of the $BaBiO_3$ structures. In refinements of the rhombohedral structure in particular we found alternate

Table 1
Details of the four distinct structures of $BaBiO_3$ ($Ba_2Bi^{3+}Bi^{5+}O_6$).

Anisotropic displacement parameters, U^{ij}, are given in units of 10^{-2} Å^2.

Atom	x	y	z	U_{iso}/U^{11}	U^{22}	U^{33}	U^{12}	U^{13}	U^{23}
T = 4.2 K, space group $P2_1/n$, a = 6.17410 (7), b = 6.12484 (7), c = 8.65220 (9) Å, β = 90.269 (1)°									
Ba	0.5045 (3)	−0.0130 (4)	0.2493 (3)	0.37 (3)					
Bi^{III}	0	0	0	0.49 (4)					
Bi^{V}	0	0	0.5	0.72 (4)					
O1	0.0689 (2)	0.0068 (4)	0.2613 (2)	0.96 (8)	0.91 (10)	1.08 (9)	−0.10 (11)	−0.09 (8)	0.09 (18)
O2	0.2465 (3)	0.2735 (4)	−0.0365 (2)	1.3 (1)	1.0 (2)	1.5 (2)	0.19 (13)	−0.31 (10)	−0.04 (12)
O3	0.2778 (3)	0.7584 (4)	−0.0371 (3)	1.1 (1)	1.6 (2)	0.77 (20)	0.48 (13)	0.01 (10)	0.17 (12)
T = 200 K, space group $I2/m$, a = 6.18505 (7), b = 6.13219 (7), c = 8.6585 (1) Å, β = 90.229(1)°									
Ba	0.5034 (3)	0	0.2490 (3)	0.99 (3)					
Bi^{III}	0	0	0	0.83 (4)					
Bi^{V}	0	0	0.5	0.90 (4)					
O1	0.0665 (2)	0	0.2611 (2)	1.5 (1)	2.5 (1)	1.5 (1)	0	−0.1 (1)	0
O2	0.2623 (2)	0.2580 (3)	−0.0355 (1)	2.1 (1)	2.3 (1)	2.0 (1)	−0.8 (1)	−0.3 (1)	0.0 (1)
T = 498 K, space group $R\bar{3}$, a = 6.1798 (1), c = 15.0453 (3) Å									
Ba	0	0	0.2526 (4)	2.3 (1)					
Bi^{III}	0	0	0	1.5 (1)					
Bi^{V}	0	0	0.5	1.8 (1)					
O	0.5402 (3)	−0.0124 (6)	0.2461 (3)	4.1 (3)	3.8 (1)	4.3 (1)	1.8 (2)	−0.8 (2)	−1.7 (1)
T = 893 K, space group $Fm\bar{3}m$, a = 8.7759 (2) Å									
Ba	0.25	0.25	0.25	4.3 (1)					
Bi^{III}	0	0	0	2.9 (1)					
Bi^{V}	0.5	0.5	0.5	2.4 (1)					
O	0.2607 (2)	0	0	3.5 (1)	10.4 (1)	= U^{22}	0	0	0

solutions characterized by octahedra of very nearly equal size. These solutions, with both Bi—O bond lengths at *ca* 2.2 Å, were rejected as unreasonable, since these bond lengths were found to be *ca* 2.3 and 2.1 Å in the high-temperature cubic phase where there were no complications from tilting, and about the same at very low temperatures where the greater distortion (see §3.2) makes for more reliable results. In effect, when ambiguities arose, we applied a criterion of distinct bond lengths in the different octahedra to select the appropriate solution.

Previous refinements of the room-temperature structure (*I*2/*m*) may have been afflicted by similar problems. Whereas Cox & Sleight (1976*a*,*b*) found the average Bi—O bond lengths to be distinctly different in the two octahedra (2.283 and 2.126 Å), and likewise Thornton & Jacobson (1978; 2.263 and 2.140 Å), Chaillout *et al.* (1985) reported essentially equal bond lengths (2.201 and 2.187 Å). In a subsequent neutron powder diffraction study of 11 different samples at room temperature (Chaillout *et al.*, 1988) seven instances of distinctly different bond lengths and four of essentially equal bond lengths were found. We suggest here that this variation may have been due not to the differences in sample preparation as Chaillout *et al.* (1988) proposed, but simply to vagaries of the refinements.

In the case of Ba_2BiSbO_6 the contrast between the cations, the size difference between the BiO_6 and SbO_6 octahedra, and out-of-phase octahedral tilting when present, all contribute intensity at the *R* points. The structural refinements were generally less troublesome, however, possibly because of a greater difference between the two bond lengths, the average Bi—O again being about 2.3 Å but Sb—O being just less than 2.0 Å. Refinements of the rhombohedral structure were occasionally problematic, but false solutions were easily recognized from unreasonable (*i.e.* equal) bond lengths and discarded.

We have just outlined problems in determining bond lengths in the face of strong contributions to the same superlattice peaks from octahedral tilting. That the octahedral tilting contributions are relatively strong suggests few problems are to be anticipated in deriving the octahedral tilt angles from the patterns recorded.

3. Results

The Rietveld method was used as outlined above to determine lattice parameters and internal coordinates in every case. In §3.1 we present a full description of each of the different structures (seven in all) encountered in this work. The data have been derived from patterns recorded for longer counting times, except those for the cubic structures, since no long counting times were employed in the pertinent temperature ranges. The measurements in fine temperature intervals, but for shorter counting times, were undertaken so we could follow the phase transitions in detail. The results are summarized *via* the lattice parameters (see §3.2), bond lengths (see §3.3) and by the manner in which the octahedral tilt angles (derived from internal coordinates) vary with temperature (see §3.4).

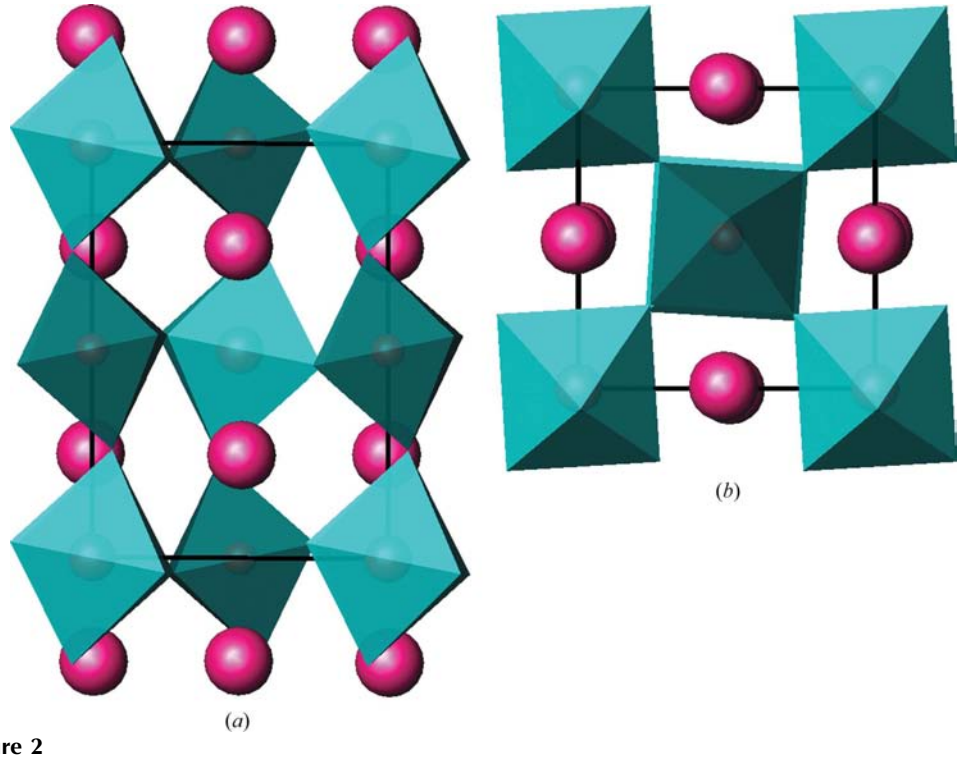

Figure 2
Representation of the low-temperature structure of $Ba_2Bi^{3+}Bi^{5+}O_6$. The spheres represent Ba while the BiO_6 groups are shown as octahedra, these octahedra being lighter and darker accordingly as they contain the larger Bi^{3+} or smaller Bi^{5+} ions, respectively. The two views shown are along the *y* and *z* axes of the monoclinic structure, these being the axes about which octahedral tilting occurs. The figures were prepared using *ATOMS* version 5.0.7, © Eric Dowty (1999).

3.1. The structures

3.1.1. $BaBiO_3$. Details of the structures at four different temperatures, corresponding to the four distinct phases of $BaBiO_3$, are recorded in Table 1.[2] The corresponding patterns have been presented in Fig. 1.

The low-temperature monoclinic structure, here at 4.2 K, has been solved and refined for the first time and is depicted in Fig. 2. The space group is $P2_1/n$ and the tilt system $a^-a^-c^+$. The views in Figs. 2(*a*) and (*b*) are constructed to highlight the tilting around an axis in the *y* direction, the $[110]_p$ direction (where subscript *p* refers to the parent structure) and in-phase tilting around an axis parallel to *z*, that is $[001]_p$, respectively. The Bi—O bond lengths in the larger $Bi^{3+}O_6$ octahedron are 2×2.299, 2×2.286, 2×2.289 Å, giving an average length of 2.291 Å, while bond lengths in the $Bi^{5+}O_6$ octahedron are 2×2.111, 2×2.114, 2×2.118 Å, giving on average 2.114 Å. The bond-valence sums (Brown & Altermatt, 1985) at the Bi ion, based on these bond lengths, are 3.5 and 5.2 in the larger and smaller octahedra, respectively. The tilt angles of the larger (smaller) octahedron about the *y* axis are approximately 11° (12°), and the tilts around the *z* axis approximately 3.5° (3.8°). More details on the calculation of these tilt angles will be given in §3.4 below.

For the second monoclinic phase, the space group is $I2/m$ and the tilt system $a^-a^-c^0$. Details of the structure at 200 K are recorded in Table 1. The space group is as reported previously for $BaBiO_3$ at room temperature and the coordinates shown in Table 1 are in most cases as previously reported, within the combined errors. The slightly odd result is that from Chaillout *et al.* (1985), who show *y*(O2) as 0.2389 (7), whereas we find this to be 0.2580 (3), in better agreement with results from other studies. The Bi—O bond lengths in the larger $Bi^{3+}O_6$ octahedron are 2×2.296 and 4×2.288 Å, averaging 2.291 Å, while bond lengths in the $Bi^{5+}O_6$ octahedron are 2×2.110 and 4×2.111 Å, with an average of 2.111 Å. The size difference is similar to that found by Cox & Sleight (1976*a*), Thornton & Jacobson (1978) and Pei *et al.* (1990), although, as already mentioned in §2, Chaillout *et al.* (1985) failed to find any such difference. The tilt angles of the larger (smaller) octahedron about the *y* axis, direction $[110]_p$ are approximately 10.5° (11.5°).

For an ordered double perovskite with rhombohedral symmetry the space group is $R\bar{3}$ and the tilt system $a^-a^-a^-$. With the coordinates as recorded in Table 1, the Bi—O bond lengths in the two octahedra are 6×2.287 and 6×2.112 Å, and the tilt angles around the threefold axis, in the $[111]_p$ direction, are 8.9 and 9.5°, respectively. These results can be compared with those from two previous measurements on the rhombohedral structure, at 419 K by Cox & Sleight (1979), and at 473 K by Pei *et al.* (1990) – these previous results can be summarized as showing a bond-length difference of 0.15 Å and a tilt angle of 9.1°. The results we obtained at 498 K are in good agreement with these. This was, however, the phase for which the refinements were the most problematic. It was clearly necessary to allow for anisotropic oxygen displacement parameters, yet this so increased the number of parameters that refinements were susceptible to giving false results. Following Cox & Sleight (1979) we noted that the inequality of the Bi—O bond lengths implies the space group $R\bar{3}$ rather than $R\bar{3}c$ and sought direct evidence for the former space-group symmetry. Cox & Sleight (1979) found this in the form of a very weak $\frac{1}{2}(111)_p$ reflection, not allowed in $R\bar{3}c$. In our

[2] Supplementary data for this paper are available from the IUCr electronic archives (Reference: WS5040). Services for accessing these data are described at the back of the journal.

Table 2
Details of the three distinct structures of Ba_2BiSbO_6.

The presentation of results is as in Table 1.

Atom	x	y	z	U_{iso}/U^{11}	U^{22}	U^{33}	U^{12}	U^{13}	U^{23}
T = 4.2 K, space group $I2/m$, a = 6.0678 (1), b = 6.0186 (1), c = 8.5082 (2) Å, β = 90.216 (1)°									
Ba	0.5023 (4)	0	0.2486 (4)	0.47 (3)					
Bi^{III}	0	0	0	0.28 (4)					
Sb^{V}	0	0	0.5	1.1 (1)					
O1	0.0513 (3)	0	0.2686 (3)	0.64 (10)	1.6 (2)	1.1 (1)	0	−0.04 (11)	0
O2	0.2698 (2)	0.2659 (3)	−0.0270 (2)	1.0 (1)	1.7 (1)	0.75 (8)	−0.04 (6)	−0.69 (6)	0.13 (10)
T = 325 K, space group $R\bar{3}$, a = 6.0572 (1), c = 14.7813 (2) Å									
Ba	0	0	0.2510 (2)	1.3 (2)					
Bi^{III}	0	0	0	0.91 (4)					
Sb^{V}	0	0	0.5	1.2 (1)					
O	0.5196 (2)	−0.0240 (2)	0.2438 (1)	3.2 (1)	2.2 (1)	2.3 (1)	1.4 (1)	−0.66 (11)	−0.83 (5)
T = 570 K, space group $Fm\bar{3}m$, a = 8.57933 (2) Å									
Ba	0.25	0.25	0.25	2.9 (1)					
Bi^{III}	0	0	0	2.4 (1)					
Sb^{V}	0.5	0.5	0.5	2.3 (1)					
O	0.2686 (2)	0	0	3.0 (1)	6.1 (1)	= U^{22}	0	0	0

case, this was recorded only in the low-angle low-resolution detector bank, where it was difficult to distinguish from the background. At 498 K, however, we were able to resolve peaks in the $\frac{1}{2}(331)_p$ group and found the intensity in the 107 reflection – hexagonal indices – that is also forbidden in $R\bar{3}c$.

Structural refinements in the cubic phase, space group $Fm\bar{3}m$, were relatively straightforward, and the results at 893 K have been included in Table 1. Oxygen displacement parameters were found to be strongly anisotropic. The R-point reflections, although weak, arise entirely from the difference in size of the octahedra, so here the estimates of the two distinct Bi—O bond lengths, 2.288 (2) and 2.100 (2) Å, can be considered reliable.[3]

3.1.2. Ba_2BiSbO_6. The chemically ordered double-perovskite Ba_2BiSbO_6 adopts just three structures, corresponding to the higher-temperature structures of $BaBiO_3$. Details at three temperatures, selected to show the three distinct structures, are shown in Table 2.

The Bi—O and Sb—O bond lengths are in all structures close to 2.31 and 1.99 Å, respectively. The difference between larger and smaller octahedra is a little larger than in $BaBiO_3$, consistent with the fact that the Sb^{5+} ion is smaller than the Bi^{5+} ion it replaces. Bond-valence sums are approximately 3.4 and 5.1 at the Bi^{3+} and Sb^{5+} ions. The octahedral tilt angles are, however, less than in $BaBiO_3$, owing to the average size of the B-site cations being smaller than in $BaBiO_3$. For the BiO_6 octahedron these angles are 8.1 and 6.7° at 4.2 and 325 K, respectively.

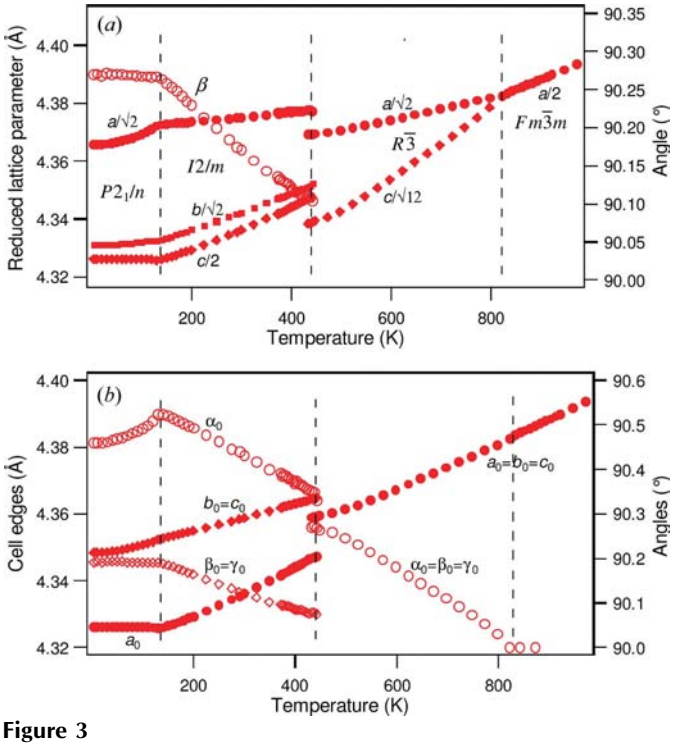

Figure 3
Temperature dependence of the lattice parameters of $BaBiO_3$. In (*a*) these parameters have been simply scaled to compare with the edge of the primitive cubic parent subcell, whereas in (*b*) they are presented *via* the dimensions of that pseudo-cubic subcell as it appears in the final structure. In both presentations the three transitions are clearly seen. At temperatures around 430 K we saw mixtures of the monoclinic $I2/m$ and rhombohedral $R\bar{3}$ phases, indicative of the first-order nature of the corresponding transition, and were able to obtain lattice parameters in both phases.

3.2. Temperature dependence of lattice parameters

Structural phase transitions are almost invariably accompanied by spontaneous strain, impacting directly on the lattice parameters and their variation with temperature (Carpenter *et al.*, 1998). Conversely, the temperature dependence of the lattice parameters is expected to reveal the occurrence of

[3] Apart from any corrections that might be necessary as a result of the strongly anisotropic vibrations just mentioned.

phase transitions and may indicate their nature. This indeed proves to be the case here.

3.2.1. $BaBiO_3$. The results for the lattice parameters of $BaBiO_3$ are presented in Fig. 3. Fig. 3(*a*) shows the lattice parameters in all phases, scaled to compare with the cell edge of the ABX_3 perovskite – this scaling is based on the nominal relationship of the lattice vectors in the pertinent subgroup with the lattice vectors of the perovskite aristotype, in $Pm\bar{3}m$ (Howard *et al.*, 2003). It can be seen that the continuous, perhaps even subtle, transition from the primitive (space group $P2_1/n$, tilt system $a^-a^-c^+$) to the body-centred monoclinic phase ($I2/m$, $a^-a^-c^0$) has a dramatic impact on the trend of the lattice parameters, notably *a*, *c* and the monoclinic angle β. The lattice parameter data of Pei *et al.* (1990), although recorded only at 50 K temperature intervals, can be recognized as being consistent with our results. The first-order transition to the rhombohedral phase ($R\bar{3}$, $a^-a^-a^-$) at *ca* 430 K is also evident (there is a two-phase region involved) and there is a continuous transition to cubic ($Fm\bar{3}m$, $a^0a^0a^0$) at *ca* 830 K. The volume per formula unit, however, varies rather smoothly through the whole temperature range, showing no readily discernable discontinuity at the first order $I2/m$ to $R\bar{3}$ transition. The connection of the unit cell of each structure to the pseudo-cubic subcell, used for purposes of scaling in Fig. 3(*a*), can also be used to derive the precise dimensions of this subcell in every case. The pseudo-cubic parameters thus obtained, in Fig. 3(*b*), represent a physically more meaningful way of describing the distortions occurring as a function of temperature. Again, three transitions can be seen.

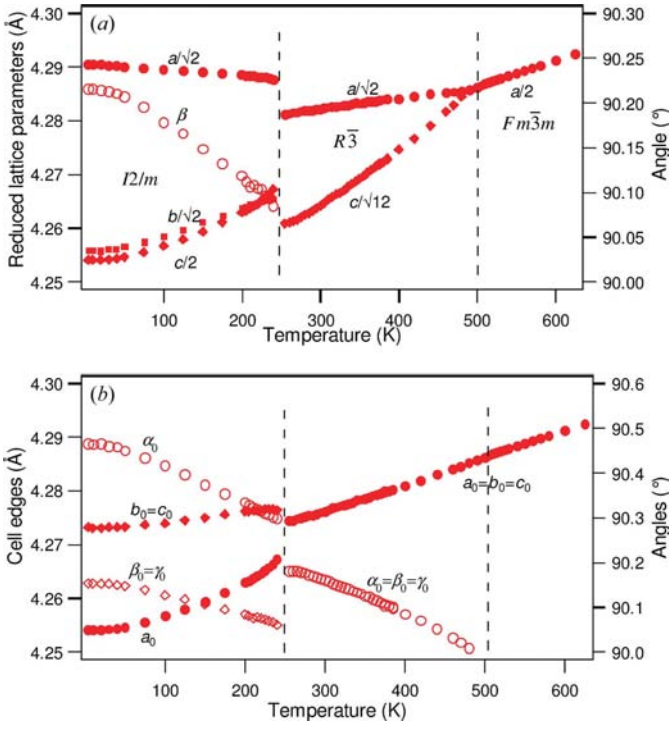

Figure 4
Temperature dependence of the lattice parameters of Ba_2BiSbO_6. Scaled lattice parameters, and the dimensions of the pseudo-cubic subcell, are shown in (*a*) and (*b*), respectively. Two transitions can be seen. At temperatures around 250 K we saw mixtures of the monoclinic $I2/m$ and $R\bar{3}$ rhombohedral phases, but attempts to refine as two-phase mixtures were in this case unsuccessful.

3.2.2. Ba_2BiSbO_6. Fig. 4 shows the temperature dependence of the lattice parameters in Ba_2BiSbO_6, presented both as suitably scaled lattice parameters (Fig. 4*a*), and *via* the parameters of the pseudo-cubic subcell. These data provide evidence for just two phase transitions in the temperature range of the study, the transition temperatures being lower than in $BaBiO_3$, and there being no sign of development of the $P2_1/n$ structure encountered in BaBiO3 below 130 K.[4] In most other respects, the data closely resemble those from $BaBiO_3$.

3.3. Bond lengths

3.3.1. $BaBiO_3$. Despite certain vagaries of the refinements as detailed earlier, we are of the view that the mean Bi—O bond lengths in the $Bi^{3+}O_6$ and $Bi^{5+}O_6$ octahedra are essentially temperature independent, at 2.29 and 2.11 Å, respectively.

3.3.2. Ba_2BiSbO_6. The mean Bi—O and Sb—O bond lengths are 2.31 and 1.99 Å, respectively, independent of temperature.

3.4. Tilt angles

The most characteristic feature of the perovskites studied here, aside from *B*-site cation ordering, is the tilting of the $(B,B')O_6$ octahedra. The tilt angles, being derived from O-atom coordinates, provide a convenient summary of results.

The first remark to be made is that there are two distinct octahedra, BO_6 and $B'O_6$, and therefore two different tilt angles (except in the cubic phase). Both tilt angles, however, are determined by the movement of the same O atom, and this implies that the tilt angles in the BO_6 and $B'O_6$ octahedra are not independent, but related in the inverse ratio of the B—O and B'—O bond lengths. To the extent that these bond lengths are constant, the tilt angles will be in a fixed ratio; this has been confirmed from our data. It suffices, therefore, to present just one of these tilt angles – we choose the smaller angle as it applies to the tilt of the larger octahedron. The second remark concerns the possibility of obtaining more than one estimate for the tilt angle of a particular octahedron – this does not apply in the case of the rhombohedral structure, but for the monoclinic structure in $I2/m$, for example, the tilt angle can be estimated from either the position of the apical oxygen O1 or the equatorial oxygen O2. The estimates obtained are very similar, as they should be (in the absence of shearing), and their average is presented here.

We show an example calculation of the tilt angle, in the $R\bar{3}$ structure. The tilt axis is $[111]_p$, which is the *z* axis in the hexagonal setting, and we consider the octahedron centred on Bi^{3+} (the larger cation) located at the origin. Table 1 shows Bi^{5+} located at $0, 0, \frac{1}{2}$, and O at 0.5402, −0.0124, 0.2461 (near $\frac{1}{2}, 0, \frac{1}{4}$). We focus on the octahedron at the origin by considering the O at $\frac{2}{3} - x(\mathrm{O}), \frac{1}{3} - y(\mathrm{O}), \frac{1}{3} - z(\mathrm{O})$ (near $\frac{1}{6}, \frac{1}{3}, \frac{1}{12}$) then the Bi^{5+}

[4] Although the lattice parameters, Fig. 4, show a degree of 'flattening' at low temperatures, it is in this case no more than to be expected from low-temperature saturation effects.

Table 3
Formulae for tilt angle calculations.

The tilt is calculated for the larger $Bi^{3+}O_6$ octahedron only. The coordinates correspond to those listed in Tables 1 and 2.

Structure, space group	Tilt axis	Expressions for tilt angle
Cubic, $Fm\bar{3}m$		No tilting
Rhombohedral, $R\bar{3}$	$[111]_p$	$\cos\varphi = \frac{3^{1/2}}{2}\frac{[1/3-y(O)]}{\{[2/3-x(O)]^2+[1/3-y(O)]^2-[2/3-x(O)][1/3-y(O)]\}^{1/2}}$
Monoclinic, $I2/m$	$[110]_p$	$\tan\varphi = \frac{x(O1)a}{z(O1)c} - (\beta-\pi/2) \simeq \frac{x(O1)}{z(O1)}/2^{1/2}$
		$\tan\varphi = -\frac{z(O2)c}{x(O2)a} \simeq -\frac{z(O2)}{x(O2)}2^{1/2}$
Monoclinic, $P2_1/n$	$[110]_p$	$\tan\varphi = \frac{x(O1)a}{z(O1)c} - (\beta-\pi/2) \simeq \frac{x(O1)}{z(O1)}/2^{1/2}$
		$\tan\varphi = -\frac{[z(O2)+z(O3)]c}{[x(O2)+x(O3)]a} \simeq -\frac{[z(O2)+z(O3)]}{[x(O2)+x(O3)]}2^{1/2}$
	$[001]_p$	$\tan\varphi = \frac{y(O2)b-x(O2)a}{y(O2)b+x(O2)a} \simeq \frac{y(O2)-x(O2)}{y(O2)+x(O2)}$
		$\tan\varphi = \frac{x(O3)a-[1-y(O3)]b}{x(O3)a+[1-y(O3)]b} \simeq \frac{x(O3)-[1-y(O3)]}{x(O3)+[1-y(O3)]}$

at $\frac{1}{3}, \frac{2}{3}, \frac{1}{6}$. Clearly, were the O to be located at $\frac{1}{6}, \frac{1}{3}, \sim\frac{1}{12}$, it would project onto the line joining Bi^{3+} and Bi^{5+}, and the tilt angle would be zero. In the tilted structure it is located at x',y',z', where $x' = \frac{2}{3} - x(O)$, $y' = \frac{1}{3} - y(O)$, $z' = \frac{1}{3} - z(O)$, and the tilt angle φ is the angle between the projections of the Bi^{3+}—O bond and the line joining Bi^{3+} to Bi^{5+}, given according to the cosine rule by

$$\cos\varphi = \frac{3^{1/2}}{2}\frac{y'}{(x'^2+y'^2-x'y')^{1/2}}.$$

Formulae used for estimating tilt angles in the different structures are recorded in Table 3.

3.4.1. $BaBiO_3$. The temperature variation of tilt angle(s) for the larger octahedron in $BaBiO_3$, estimated as explained above, is displayed in Fig. 5. A notable feature apparent in this figure is that the magnitude of the tilt angle changes very little as, at the $I2/m$ to $R\bar{3}$ transition, the tilt axis switches discontinuously from $[110]_p$ to $[111]_p$. We have noted similar remarkable behaviour in analogous transitions, such as at the first-order *Imma* to $R\bar{3}c$ transition in $PrAlO_3$ (Carpenter *et al.*, 2005). That the tilt angle φ (out-of-phase tilting) varies continuously through the continuous $P2_1/n$ to $I2/m$ transition is not unexpected, although the data suggest a flatter trend through the $P2_1/n$ phase as the in-phase tilting takes effect.

The nature of the each continuous transition in $BaBiO_3$ can be investigated by taking the tilt angle(s) to represent the order parameter(s) in the different phases. We have found the variation of the tilt angle φ to be well described by $\varphi^4 \propto (T_c - T)$, $T_c = 820$ K, through both the $I2/m$ and $R\bar{3}$ phases, corresponding to a transition to cubic tricritical in nature (Salje, 1990). The variation of ψ is better described by $\psi^4 \propto \Theta_s(\coth\frac{\Theta_s}{T_c} - \coth\frac{\Theta_s}{T})$, $T_c = 132$ K, $\Theta_s = 35$ K, the modification to the right-hand side accounting for saturation effects at lower temperatures (Salje *et al.*, 2005). The dashed curves shown in Fig. 5 are calculated on the basis of these fits.

3.4.2. Ba_2BiSbO_6. The tilt angle for the BiO_6 octahedron is shown in Fig. 6. We note that in this compound also, the magnitude of the tilt varies in a nearly continuous manner through the first-order $I2/m$ to $R\bar{3}$ transition. A plot of φ^2 *versus* temperature was nearly linear, but adding a quadratic term gave a better fit. We attribute the nonlinearity as a contribution from the Q^6 term in the free-energy expansion, and indeed we could fit the temperature variation with a function of the form $\varphi^2 \propto [1 + k(T_c - T)]^{1/2} - 1$, $T_c = 515$ K, $k = 0.0232$, as appropriate in this case (Ballaran *et al.*, 2000).

4. Summary and discussion

High-resolution neutron powder diffraction has been used to investigate the structures and phase transitions in $BaBiO_3$ and Ba_2BiSbO_6. Charge ordering in $BaBiO_3$ has been confirmed. The structure of the low-temperature phase of $BaBiO_3$ has

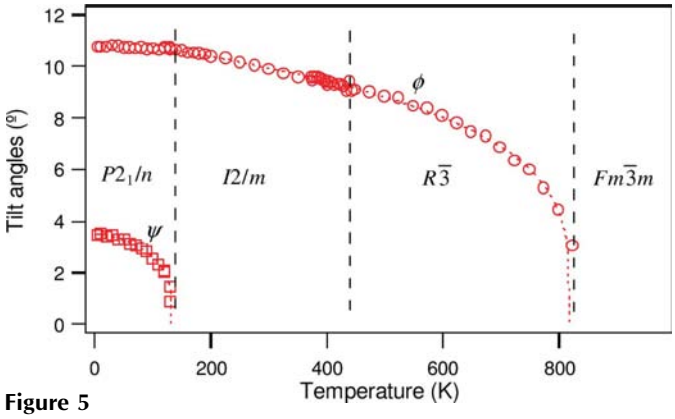

Figure 5
Temperature dependence of the in-phase and out-of-phase tilt angles, ψ and φ, for $BaBiO_3$. The apparent continuity of φ through the discontinuous $I2/m$ to $R\bar{3}$ phase transition is a notable feature. The fitted curves (dashed lines) correspond to phase transitions tricritical in nature.

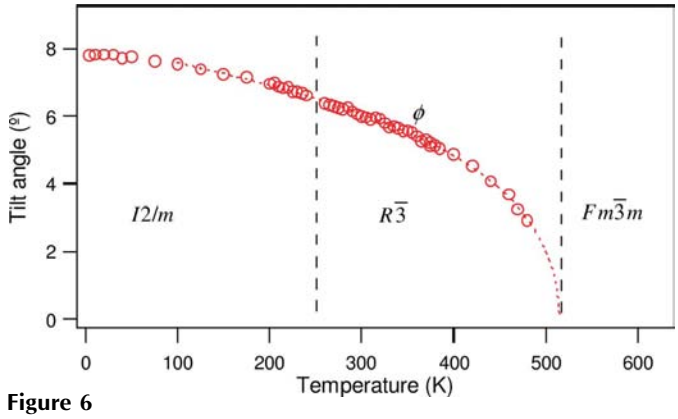

Figure 6
Temperature dependence of the tilt angle φ in Ba_2BiSbO_6. The dashed line, given by $\varphi^2 = 25.36\{[1+0.0232(T_c - T)]^{1/2} - 1\}$, $T_c = 514.9$ K, is of the form to be expected when the sixth order term of the free energy expansion is included in the analysis.

been confirmed as monoclinic, in the space group $P2_1/n$, as suggested by Howard *et al.* (2003) on the basis of an earlier report of its existence (Pei *et al.*, 1990). This phase does not occur in Ba_2BiSbO_6. Lattice parameters precisely determined at fine temperature intervals show all the phase transitions quite clearly.

Structure refinements based on data recorded in relatively short runs were sometimes problematic, particularly in the rhombohedral phase of $BaBiO_3$. In some cases it was difficult to determine with adequate precision the lengths of the Bi—O bonds. We now believe some previous findings of the absence of charge ordering in $BaBiO_3$ may be attributed to vagaries in the structure refinements. We believe nonetheless that our own refinements are adequate in this respect and that the (mean) bond lengths in the larger and smaller octahedra in $BaBiO_3$ are 2.29 and 2.11 Å, essentially independent of temperature over the temperature range (4.2–973 K) of this study. In Ba_2BiSbO_6 the corresponding bond lengths, for Bi—O and Sb—O, are 2.31 and 1.99 Å, respectively, independent of temperature.

There are many similarities in behaviour between the charge-ordered double perovskite $BaBiO_3$ and the chemically ordered compound Ba_2BiSbO_6. The differences can be attributed, at least qualitatively, to the fact that the Sb^{5+} ion is smaller than the Bi^{5+} ion. Specifically, the smaller size of the Sb^{5+} ion accounts for the smaller (1.99 *versus* 2.11 Å) bond lengths in the smaller of the $B(B')O_6$ octahedra in Ba_2BiSbO_6, while the smaller average size of the *B*-site cations leads to smaller tilt angles (§3.4) and less distortion (§3.2). This leads to transition temperatures in Ba_2BiSbO_6 that are lower than the temperatures for the corresponding transitions in $BaBiO_3$. The lowest temperature transition in $BaBiO_3$ has no analogue in Ba_2BiSbO_6, the smaller tilt angle in Ba_2BiSbO_6 evidently being accommodated without the need for tilting around a second axis. Bond-valence sums are roughly 3.5 for the larger Bi, and 5.1 for both the smaller Bi and Sb. The value of 5.1 for Bi^{5+} and Sb^{5+} is quite satisfactory – the value of 3.5 for Bi^{3+} perhaps less so, but is consistent with findings from previous studies (Cox & Sleight, 1976*a*; Thornton & Jacobson, 1978).

Octahedral tilt angles have been derived from refined internal coordinates. A notable feature is the near continuity of the magnitude of the tilt angle (φ) as the tilt axis switches discontinuously from $[110]_p$ to $[111]_p$. Taking the tilt angle(s) to represent the order parameter(s) we find in $BaBiO_3$ that both the $P2_1/n$ to $I2/m$ and $R\bar{3}$ to $Fm\bar{3}m$ transitions are tricritical in nature. The transition in Ba_2BiSbO_6 is closer to second order, although with a probable contribution from the sixth order term in the free-energy expansion. We are unsure of the reason for this difference, although it could be related simply to the existence of the additional low-temperature phase in $BaBiO_3$.

We have undertaken limited analysis of the spontaneous strains occurring and our final comment concerns the connection between the rhombohedral distortion in $R\bar{3}$ and the order parameter as represented (we propose) by the tilt angle φ shown above. The rhombohedral distortion, e_4, is closely approximated (Carpenter *et al.*, 2005) by the difference from $\pi/2$ of the angle in the pseudo-cubic subcell, as displayed in Figs. 3(*b*) and 4(*b*). Since the symmetry of this distortion (irreducible representation Γ_5^+ of the space group $Fm\bar{3}m$) differs from that driving the transition (active irrep Γ_4^+), we expect $\alpha_0 - \pi/2 \propto \varphi^2$ (Carpenter *et al.*, 1998). Plots of φ^2 *versus* α_0 are shown in Fig. 7. Although the variation of φ^2 with α_0 is reasonably linear, the lines intercept the axis (at $\pi/2$) at values distinctly different from zero. One possibility is that the non-zero intercept represents some average angle of dynamical tilting at the transition to the cubic phase. We have also noticed that the data seem to be better described by $\alpha_0 = \pi/2 \propto \varphi^3$, but we know of no reason why such a relationship should pertain.

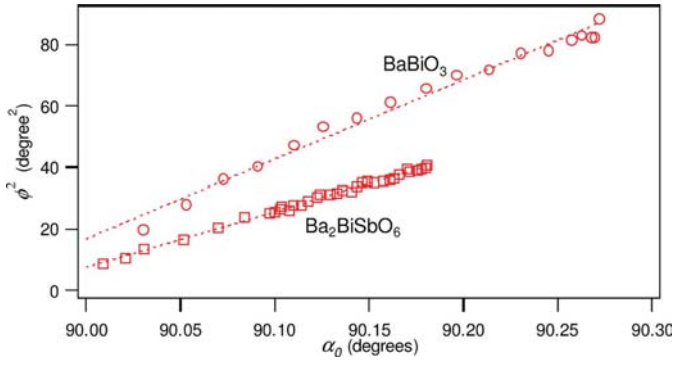

Figure 7
Relationship of rhombohedral strain, represented by $\alpha_0 - \pi/2$, to the square of the order parameter, represented by φ^2. The relationship may be linear, but the lines do not intercept zero at $\alpha_0 = \pi/2$.

We thank Professor Michael Carpenter, University of Cambridge, for his interest in these systems, and his assistance in the analysis of spontaneous strains. The neutron facilities at ISIS are operated by the Council for the Central Laboratory of the Research Councils (CCLRC), with a contribution from the Australian Research Council. Travel funding to ISIS, for BJK, CJH and ZZ, was provided by the Access to Major Research Facilities Program operated by the Commonwealth of Australia. The studies of perovskites are supported by the Australian Research Council, grant DP0557222.

References

Ballaran, T. B., Angel, R. J. & Carpenter, M. A. (2000). *Eur. J. Mineral.* **12**, 1195–1213.
Brown, I. D. & Altermatt, D. (1985). *Acta Cryst.* B**41**, 244–247.
Carpenter, M. A., Howard, C. J., Kennedy, B. J. & Knight, K. S. (2005). *Phys. Rev. B*, **72**, 024118/1–15.
Carpenter, M. A., Salje, E. K. H. & Graeme-Barber, A. (1998). *Eur. J. Mineral.* **10**, 621–691.
Cava, R. J., Batlogg, B., Krajewski, J. J., Farrow, R. C., Rupp, L. W., White, A. E., Short, K. T., Peck, W. F. & Kometani, T. Y. (1988). *Nature*, **332**, 814–816.
Chaillout, C., Remeika, J. P., Santoro, A. & Marezio, M. (1985). *Solid State Commun.* **56**, 829–831.
Chaillout, C., Santoro, A., Remeika, J. P., Cooper, A. S., Espinosa, G. P. & Marezio, M. (1988). *Solid State Commun.* **65**, 1363–1369.
Cox, D. E. & Sleight, A. W. (1976*a*). *Solid State Commun.* **19**, 969–973.

Cox, D. E. & Sleight, A. W. (1976*b*). *Proceeding of Conference on Neutron Scattering*, edited by R. M. Moon, pp. 45–54, Gatlinburg, Tennessee; available from the National Technical Information Service, Springfield, VA 22161, USA.
Cox, D. E. & Sleight, A. W. (1979). *Acta Cryst.* B**35**, 1–10.
Dowty, E. (1999). *ATOMS*, Version 5.0.7. Shape Software, Kingsport, Tennessee, USA.
Howard, C. J., Kennedy, B. J. & Woodward, P. M. (2003). *Acta Cryst.* B**59**, 463–471.
Ibberson, R. M., David, W. I. F. & Knight, K. S. (1992). Rutherford Appleton Laboratory Report RAL 92–031.
Larson, A. C. & von Dreele, R. B. (2000). *GSAS: General Structure Analysis System.* Los Alamos National Laboratory Report LAUR 86–748.
Pei, S., Jorgensen, J. D., Dabrowski, B., Hinks, D. G., Richards, D. R., Mitchell, A. W., Newsam, J. M., Sinha, S. K., Vaknin, D. & Jacobson, A. J. (1990). *Phys. Rev. B*, **41**, 4126–4141.
Salje, E. H. K. (1990). *Phase Transitions in Ferroelastic and Co-elastic Crystals.* Cambridge University Press.
Salje, E. H. K., Hayward, S. A. & Lee, W. T. (2005). *Acta Cryst.* A**61**, 3–18.
Shannon, R. D. (1976). *Acta Cryst.* A**32**, 751–767.
Sleight, A. W., Gillson, J. L. & Bierstedt, P. E. (1975). *Solid State Commun.* **17**, 27–28.
Thornton, G. & Jacobson, A. J. (1978). *Acta Cryst.* B**34**, 351–354.
Toby, B. H. (2001). *J. Appl. Cryst.* **34**, 210–213.
Zhou, Q. & Kennedy, B. J. (2004). *Solid State Commun.* **132**, 389–392.